Power, Energy and Electrical Engineering
M. Deng (Ed.)

doi:10.3233/ATDE240312

Thermal Effect for Lifetime of IGBT Depend on Inertia Constant of Virtual Synchronous Generator

Keigo Higashiura [a,1] Ryuto Shigenobu [a] Akiko Takahashi [a] and Masakazu Ito [a]
[a] *Power System Laboratory, University of Fukui, Japan*

Abstract. Increasing integration of inverter power sources into the electrical power system has raised concerns about a lack of system inertia, leading to potential disturbances in system frequency and speed during grid disruptions. Virtual synchronous generator (VSG) control is a promising solution for inertia support of the electrical power system. VSG's inertia enhances system stability by eliminating small and occasional disturbances. However, the required system-wide inertia and the appropriate inertia characteristics supplied by individual VSG remain unclear. Also, the power variation in power electronic interface inverters caused by VSG control increases the stress on power semiconductor devices. In this paper, the focus is that VSG's inertia ensures grid-side stability by removing disturbances and the influence of VSG on the lifetime of power semiconductors. First, temperatures of the IGBTs are obtained from the inverter model considering the thermal model and HILs simulations with small and occasional disturbances. Next, the lifetimes of the IGBTs are calculated from the results of the rainflow analysis of these temperatures, using the linear cumulative damage theory in lifetime prediction. As a result, a trade-off relationship between system stability and IGBT lifetime is confirmed.

Keywords. grid-following inverter, virtual synchronous generator, virtual inertia, lifetime, distributed generator

1. Introduction

Need for a sustainable society and environment has led to the massive introduction of distributed generators (DGs), such as variable renewable energy sources in the electric network [1]. Power electronics inverters are widely used as the interfaces for integrating the DGs into the grid [2]. The grid frequency was traditionally regulated by synchronous generators (SGs), which can provide inertia by absorbing or transferring kinetic energy stored in rotors and turbines. On the other hand, general power electronics inverters have very small or no inertia and damping properties. Therefore, the high rate of system non-synchronous penetration (SNSP) with the massive introduction of VREs reduces the electrical system's inertia due to replacing the SGs. This could lead to instability conditions (potential disturbances in system frequency and speed during grid disruptions) compared to SG-dominated conventional systems [3, 4].

Virtual synchronous generator (VSG) control that emulates inertia and damping function has been proposed to compensate SG characteristics by an inverter. VSG control

[1] Corresponding Author, Keigo Higashiura, Power System Laboratory, University of Fukui, 3-9-1, Bunkyo, Fukui 910-8507, Japan; E-mail: higashiura.keigo@pws.fuee.u-fukui.ac.jp.

is a promising solution for inertia support of the electrical power system [5]. A notable feature of VSGs is that their parameters, such as virtual inertia constant *H* and damping constant *D*, are not constrained by physical factors in the same way as real SGs.

Traditionally, the power system's frequency is controlled to adhere to frequency management target values established in each region, ensuring the maintenance of supply-demand balance. System inertia is effective in mitigating frequency variations even for small and oscillational disturbances, and it is anticipated that the inertia of the VSG can also eliminate these disturbances [6]. However, from the view of stability and quality, the required whole system inertia and the appropriate inertia characteristics supplied by individual VSG remain unclear due to the lack of several index definitions [7].

Many DGs are supplied by power semiconductors, in particular, insulated gate bipolar transistors (IGBTs). IGBTs are the most vulnerable component in power electronic inverters [8]. Due to the difficulty of non-destructive detection of IGBT damage, it becomes essential to estimate the remaining lifetime until failure. Power processing stresses these delicate devices, affecting their lifetime and ultimately the system's reliability. In recent reliability studies, the failure of power semiconductor devices is mainly caused by thermal stress, evaluated by average junction temperature and junction temperature cycles during operating periods. In [9] and [10], it is possible to ensure the system's reliability by identifying the causes of IGBT failures and extrapolating IGBT lifetime from the thermal fatigue phenomena occurring during power processing. Also, based on the experimental verification of linear cumulative damage theories in predicting the lifetime of power semiconductor devices [11], determine these devices' Life Consumption (LC).

The power variation in power electronic interface inverters caused by VSG control increases the stress on IGBT devices. Therefore, it is necessary to consider the influence of VSG's inertia on the LC of IGBT devices. This paper proposes an approach that considers both inertia and LC from the view of stability and reliability, respectively, to design the virtual inertia constant *H* applied to VSGs. The rest of the paper is organized as follows : Section 2 reviews control methods of the VSG. Section 3 reviews a step of the lifetime calculation considering the thermal model. Section 4, 5 reviews the analysis divided into stability and reliability aspects.

2. Grid-following VSG Model

VSG control can be divided into two types of inverter control: the grid-forming (GFM) inverter and the grid-following (GFL) inverter in works of literature [12]. The GFM type, functioning as a voltage-controlled voltage source, has the capability to maintain the system's voltage and frequency, enabling autonomous operation. On the other hand, the GFL type, operating as a current-controlled voltage source, detects the phase of the system voltage through a PLL circuit and outputs the inverter's power. Consequently, it requires a reference system and cannot operate autonomously.

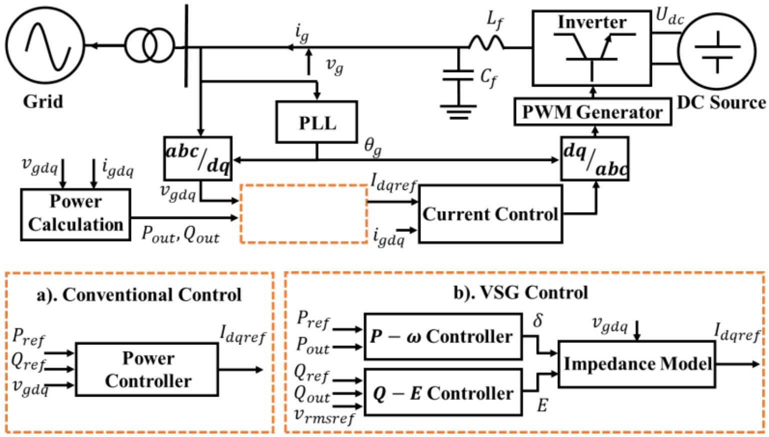

Figure 1. GFL control configuration.

a). Conventional control, b).VSG control.

Otherwise, the GFL type, compared to the GFM type, can follow the system without causing conflicts, making it capable of tracking the system. Additionally, the GFL type, widely utilized in current inverter control methods, is considered to introduce minimal disruptions when implementing control into the system. Therefore, this verification focused on validating the inverter control using the GFL type.

The general structure of GFL type is shown in Figure 1. PWM input signal was generated from the current control block. In Figure 1, U_{dc} is the DC voltage, L_f, C_f are filter inductor and filter capacitor. v_g, i_g are grid voltage and grid current, respectively. θ_{grid} is electrical system phase angle calculated from the PLL.

2.1. Conventional Control for GFL-Type.

A control method applied to a general grid-connected inverter is shown in Figure 1(a). The Power controller equation is given in (1) and (2).

$$i_{dref} = \left(P_{ref}v_{gd} + Q_{ref}v_{gq}\right)/\left(v_{gd}^2 + v_{gq}^2\right) \tag{1}$$

$$i_{qref} = \left(P_{ref}v_{gq} - Q_{ref}v_{gd}\right)/\left(v_{gd}^2 + v_{gq}^2\right) \tag{2}$$

where, P_{ref}, Q_{ref} are the active power reference and the reactive power reference, respectively.

2.2. VSG Control

The general structure of GFL-type VSG is shown in Figure 1(b). The VSG function is achieved by applying swing equation of SG virtually at the current control block. VSG consists of a *P-ω* controller imitated swing equation, a *Q-E* controller carrying out the AVR function and an impedance model for calculating the current reference.

2.2.1. *P-ω Controller* (*Virtual Inertia*)

The model of the *P-ω* controller is shown in Figure 2. Swing equation is applied to simulate an inertia equivalent to that of a SG, as expressed in (3).

$$2H \cdot \frac{d\omega_{vsg}}{dt} = P_{ref} - P_{out} - D(\omega_{vsg} - \omega_{grid}) \tag{3}$$

where P_{out} is the VSG output. H and D represent the inertia constant and the damping constant. $\omega_{vsg}, \omega_{grid}$ are the VSG virtual angular velocity, and grid angular velocity, respectively.

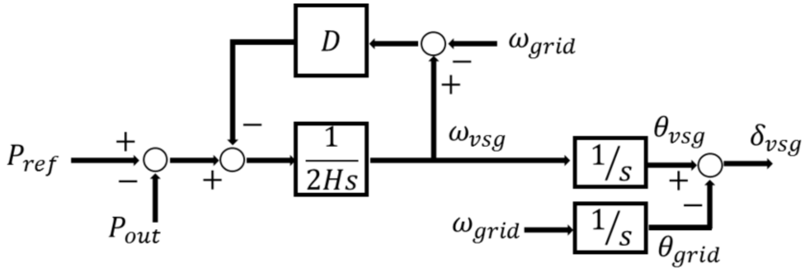

Figure 2. *P-ω* controller.

2.2.2. *Q-E Controller* (*AVR Function*)

Virtual terminal voltage E is obtained from the *Q-E* controller. *Q-E* controller equation is given in (4).

$$E = \left[(Q_{ref} - Q_{out})D_q + v_{rmsref} - v_{rms}\right]\left(k_p + \frac{k_i}{s}\right) \tag{4}$$

Q-E controller has imitated the excitation system of SG. [16] The PI control regulates the voltage signal. *Q-E* controller is represented in Figure 3. Q_{out} is the VSG reactive power output. D_q is the voltage droop constant. v_{rmsref}, v_{rms} are voltage reference and grid voltage, respectively. k_p, k_i are proportional gain and integral gain. The voltage droop control and PI control are designed to emulate SG's control and prime mover's delay.

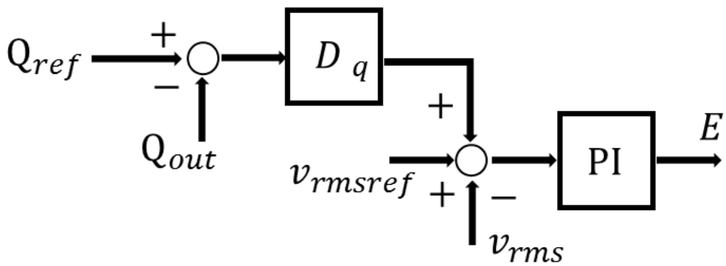

Figure 3. *Q-E* controller.

2.2.3. Impedance Model for GFL-VSG

The impedance model imitated the relation that exist between the internal EMF and terminal voltage in SG. This relation can be used to calculate the current reference. The current reference equations are indicated in (5) and (6).

The impedance model imitated the relation that exist between the internal EMF and terminal voltage in SG. This relation can be used to calculate the current reference. The current reference equations are indicated in (5) and (6).

$$I_{dref} = \frac{r}{r^2 + x^2}\left(Ecos\delta_{vsg} - v_{gd}\right) + \frac{x}{r^2 + x^2}\left(Esin\delta_{vsg} - v_{gq}\right) \tag{5}$$

$$I_{qref} = \frac{r}{r^2 + x^2}\left(Esin\delta_{vsg} - v_{gq}\right) - \frac{x}{r^2 + x^2}\left(Ecos\delta_{vsg} - v_{gd}\right) \tag{6}$$

where, r, x are virtual armature resister and virtual reactance, respectively. δ_{vsg} and E are obtained from P-ω controller and Q-E controller. The detailed impedance model was given in [16].

3. Lifetime Calculation Model

The lifetime can be calculated from the power cycling lifetime curve that expresses the relationship between the number of cycles and the temperature change as damage. The power cycling lifetime curve can be divided to two types: the power cycling lifetime curves are ΔT_j and ΔT_c. The ΔT_j curve is dominated by failure due to deterioration of the aluminum wire bonds on the chip surface when the element temperature rises and falls suddenly. On the other hand, the ΔT_c curve is dominated by failure due to deterioration of the solder joints between the insulated substrate DCB and the copper base plate, which becomes predominant when the case temperature rises and falls. This paper exclusively considers the ΔT_j curve to focus on the effects of rapid temperature changes.

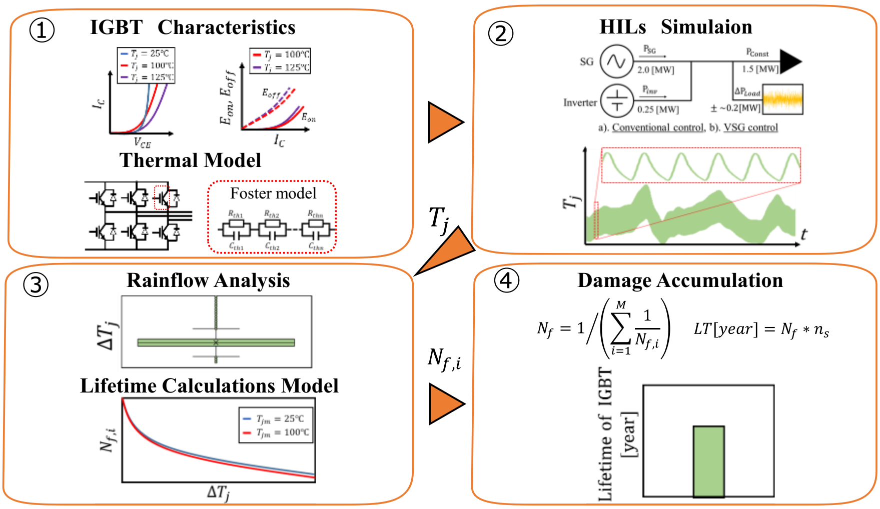

Figure 4. The steps to calculate lifetime of IGBT.

The steps to calculate lifetime of IGBT are shown in Figure 4. First, data sheet for calculating IGBT switching losses is extracted in look up table format. Also, a thermal model is created to inverter switching losses into temperature. Second, the switching losses and thermal model are embedded into the inverter for HILs simulation, and the temperature of the IGBT is measured. Third, rainflow analysis is performed on the IGBT temperature data, calculating parameters such as temperature changes. Using information derived from rainflow analysis, the number of cycles until failure is determined. Finally, based on the number of cycles until failure, the lifetime of the IGBT is calculated.

3.1. Thermal Model

The thermal model of the three-phase inverter is shown in Figure 5. The foster thermal RC network is used to model thermal changes and calculate the temperatures of IGBTs and diodes. Equations (7), (8), and (9) represent the formulas for determining the junction temperature, case temperature, and heatsink temperature, respectively.

$$T_j(t) = P_I(t) \times Z_{th(j-c)}(t) + T_C \tag{7}$$

$$T_C(t) = \left(P_I(t) + P_D(t)\right) \times Z_{th(c-f)}(t) + T_f \tag{8}$$

$$T_f(t) = P_{total}(t) \times Z_{th(f-a)}(t) + T_a \tag{9}$$

where,$P_I(t)$, $P_D(t)$ and $P_{total}(t)$ the power loss of a single IGBT, the power loss of a single Diode, and the total power losses of all of the IGBT and Diode, respectively.

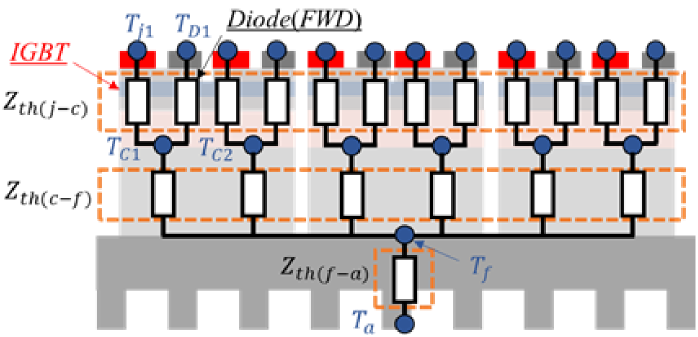

Figure 5. Thermal model for three phase inverter.
Zth(j-c): junction-to case thermal impedance, Zth(c-f): case-to-heatsink thermal impedance, Zth(f-a): heatsink-to-ambient thermal impedance, Tj: junction temperature, Tc: case temperature, Ts: heatsink temperature, Ta: ambient temperature.

3.2. Rainflow Analysis

Rainflow analysis is suitable for investigating how damage accumulates on a target object under conditions where stress changes periodically [14]. Utilizing rainflow analysis based on the irregular temperature variations obtained from HILs simulations, the amplitude of temperature changes ($\Delta T_{j,i}$), cycle period at this point ($t_{on,i}$), and average temperature ($T_{jm,i}$) are decomposed into several regular cycles.

3.3. Lifetime Consumption

According to [11], a lifetime model of a IGBT device can be given in (10)

$$N_{f,i} = A \times \left(\Delta T_{j,i}\right)^{\alpha} \times (ar)^{\beta_1 \Delta T_{j,i} + \beta_0} \times \left[\frac{C + \left(t_{on,i}\right)^{\gamma}}{C+1}\right] exp\left(\frac{E_a}{k_b \times T_{jm,i}}\right) \times f_d \quad (10)$$

where, $N_{f,i}$ is the number of cycles to failure at the respective power rise peaks. $t_{on,i}$ is cycle period, which are obtained from the rainflow cycle. $T_{jm,i}$ is mean junction temperature. Other coefficient parameters are given in Table 1.

Considering the inverter's operational time (HILs simulation time) as one operating cycle, the lifetime is consumed by different temperature changes *M* times within one operating cycle, as per (10). The total failure cycles corresponding to different *M* temperature changes within one operating cycle of the inverter, as expressed in (11).

$$N_f = 1 \Bigg/ \left(\sum_{i=1}^{M} \frac{1}{N_{f,i}}\right) \quad (11)$$

Also, the product of (11) and the total the number of cycles until failure provide the lifetime of the IGBT device as expressed in (12).

$$LT = N_f * n_s / (60 \times 60 \times 24 \times 365) \quad (12)$$

where, n_s is one cycle of operation mode (simulation time). LT is lifetime of the IGBT.

Table 1. Parameter of the lifetime model of IGBT.[10]

Parameter	Value	Experimental Condition
A	3.4368×10^{14}	
α	-4.923	$64\text{K} \leq \Delta T_j \leq 113\text{K}$
ar	0.28	
β_0	1.942	$0.19 \leq ar \leq 0.42$
β_1	-9.012×10^{-3}	
C	1.434	$0.07\text{s} \leq t_{on} \leq 63\text{s}$
γ	-1.208	
E_a	0.06606 eV	$305.6\text{K} \leq T_{jm} \leq 395.1\text{K}$
k_b	8.6173×10^{-5}eV/K	
f_d	0.6204	

4. Simulation Conditions

The system configuration and control parameters of the simulation validated in the HILs environment are shown in Figure 6 and Table 2. On the supply side, two units comprise one inverter and one SG. On the load side, there is a constant load (P_{Const}) and a small load fluctuation based on probability density distribution (ΔP_{Load}). The SG has a governor control, while the inverter does not. The active power reference P_{ref} value for the inverter remains constant at 0.20 MW. The results for system stability and lifetime are presented for both conventional methods and VSG at inertia constants $\in \{4.0, 8.0, 12.0, 16.0\}$. Only data that allows neglect of the effects of temperature rise during inverter startup were used for analysis, with simulation times n_s of 1200 [s].

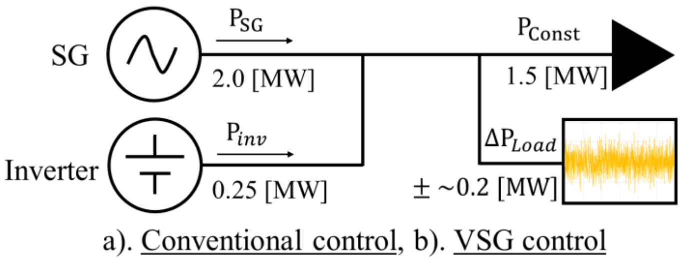

Figure 6. GFL inverter control configuration.

Table.2. Simulation parameters.

Parameters name	Variables	Values
DC-link voltage	U_{dc}	500[V]
Grid voltage (inverter side)	v_g	270[V]
Utility frequency	f_{grid}	60[Hz]
Filter inductor, capacitor	L_f, C_f	0.5 [mH],90.6[μH]
Switching frequency	f_{SW}	10.0[kHz]
Damping constant (VSG)	D	30[-]
Virtual reresister,reactance (VSG)	r, x	0.2[pu],0.4[pu]

5. Simulation Results

5.1. System Stability

The probability density distribution of the system frequency for both conventional methods and each inertia constant *H* is shown in Figure 7. From Figure 7, it is evident that VSG can suppress frequency fluctuations compared to the conventional method. Additionally, it can be observed that a larger inertia constant *H* results in better suppression of frequency variations. Therefore, the larger the inertia constant *H* of the VSG, the more it can contribute to the system stability.

Active power outputs of conventional and VSG control is shown in Figure 8. In conventional control, the setpoint of 0.2 MW is maintained. On the other hand, in VSG control, it can be observed that the active power output as an inertia response increases as the inertia constant *H* becomes larger.

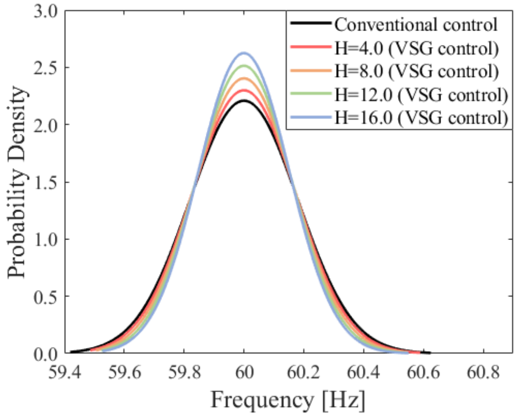

Figure 7. The probability density distribution of the system frequency.

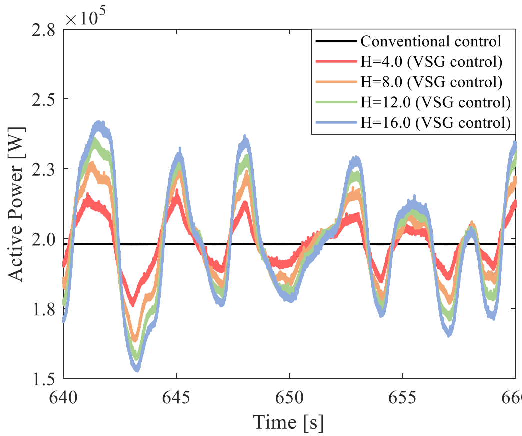

Figure 8. Active power outputs of conventional and VSG control.

5.2. Lifetime of IGBT

The IGBT junction temperature calculated from the rainflow analysis is shown in Figure 9. It is evident that as the inertia constant H increases, the junction temperature's amplitude changes, as indicated by the more extensive interquartile range. In addition, it can be observed that the values of the temperature change amplitude increase significantly for outlier cases. Also, it can be observed that the average value of the temperature change amplitude remains constant. This indicates a steady temperature rise due to switching, which is consistent with the constant active power reference value.

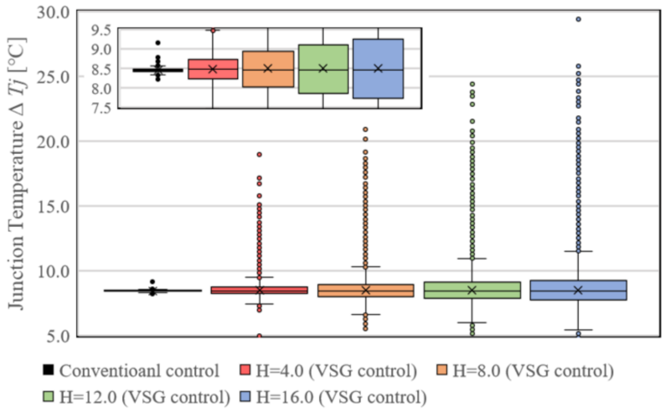

Figure 9. The IGBT junction temperature calculated from the rainflow analysis.

The cycle to failure in terms of junction temperature for IGBT under different thermal stresses is shown in Figure 10 from (10). The number of cycles to failure decreases as the average junction temperature and the amplitude of the temperature changes increase.

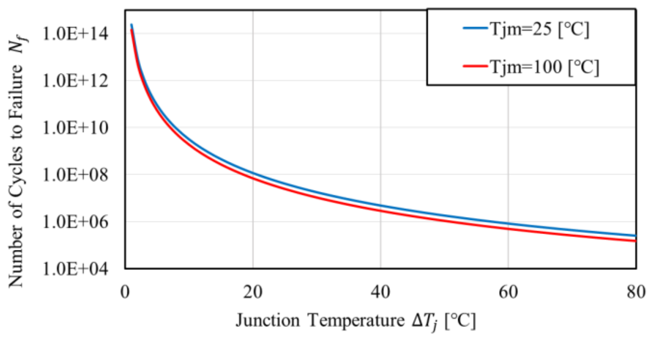

Figure 10. The number of cycles to failure for IGBT under different thermal stresses. ($t_{on} = 1[s]$)

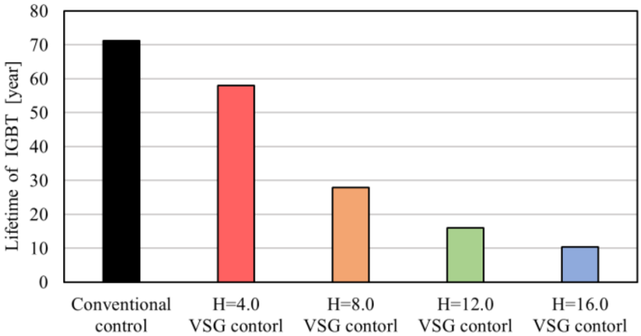

Figure 11. The IGBT lifetime based on the difference between the inertia constant (VSG control) and the conventional control.

The IGBT lifetime based on the difference between the inertia constant (VSG control) and the conventional control is shown in Figure 11. As the inertia constant *H* increases, the lifetime becomes shorter due to the more influential temperature rise, resulting in fewer cycles until failure.

6. Conclusion

The focus of this paper is on the relationship between the inertia constant *H* and the IGBT lifetime. It was confirmed that VSG suppresses disturbances by providing inertia for small and oscillational disturbances compared to conventional control methods. Moreover, increasing the inertia constant *H* of VSG allows for better suppression of frequency variations, contributing to system stability. On the other hand, supplying active power as inertia influences the junction temperature rise of IGBT due to switching losses. Additionally, it was observed that the increase in junction temperature rise affects the lifetime of IGBT. Therefore, increasing the inertia constant *H* can contribute to system stability but shortens the lifetime of IGBT. Conversely, reducing the inertia constant *H* may extend the lifetime of IGBT but compromise system stability. The relationship between system stability and IGBT lifetime was confirmed to be a trade-off.

References

[1] Li HX, Edwards DJ, Hosseini MR, Costin GP. A review on renewable energy transition in Australia: An updated depiction. Journal of Cleaner Production. 2020;242.

[2] Al-Shetwi, Ali & Sujod, Muhamad & Hannan, M. A. & Abdullahd,et al. Impact of Inverter Controller-Based Grid- Connected PV System in the Power Quality. COMPEL International Journal of Computations and Mathematics in Electrical. 2020 Dec, 10.18178/ijeetc.9.6.462-469.

[3] Tielens P, Van Hertem D. The relevance of inertia in power systems. Renewable & Sustainable Energy Reviews. 2016;55:999-1009.

[4] Ulbig, Andreas & Borsche, Theodor & Andersson, Göran. Impact of Low Rotational Inertia on Power System Stability and Operation. IFAC Proceedings Volumes (IFAC-PapersOnline). 2013. 19.

[5] Liu J, Miura Y, Ise T. Comparison of Dynamic Characteristics Between Virtual Synchronous Generator and Droop Control in Inverter-Based Distributed Generators. Ieee Transactions on Power Electronics. 2016;31(5) :3600-11.

[6] Oshnoei S, Aghamohammadi M, Oshnoei A, Mohammadi-Ivatloo B. Provision of Frequency Stability of an Islanded Microgrid Using a Novel Virtual Inertia Control and a Fractional Order Cascade Controller. Energies. 2021;14(14).

[7] Xu QW, Dragicevic T, Xie LH, Blaabjerg F. Artificial Intelligence-Based Control Design for Reliable Virtual Synchronous Generators. Ieee Transactions on Power Electronics. 2021;36(8):9453-64.

[8] Reigosa PD, Wang H, Yang YH, Blaabjerg F. Prediction of Bond Wire Fatigue of IGBTs in a PV Inverter Under a Long-Term Operation. Ieee Transactions on Power Electronics. 2016;31(10):7171-82.

[9] He JK, Sangwongwanich A, Yang YH, Iannuzzo F. Lifetime Evaluation of Three-Level Inverters for 1500-V Photovoltaic Systems. Ieee Journal of Emerging and Selected Topics in Power Electronics. 2021;9(4):4285-98.

[10] Sangwongwanich A, Yang YH, Sera D, Blaabjerg F. Mission Profile-Oriented Control for Reliability and Lifetime of Photovoltaic Inverters. Ieee Transactions on Industry Applications. 2020;56(1):601-10.

[11] Schmidt, Ralf & Newman, Paul & Scheuermann, Uwe. Power cycling testing with different load pulse durations. 7th IET International Conference on Power Electronics, Machines and Drives, PEMD 2014. 2014. 1.9.03-1.9.03. 10.1049/cp.2014.0475.

[12] Rathnayake DB, Akrami M, Phurailatpam C, Me SP, Hadavi S, Jayasinghe G, et al. Grid Forming Inverter Modeling, Control, and Applications. Ieee Access. 2021;9:114781-807.

[13] Hirase Y, Abe K, Sugimoto K, Shindo Y. A grid-connected inverter with virtual synchronous generator model of algebraic type. Electrical Engineering in Japan. 2013;184(4):10-21.

[14] Musallam M, Johnson CM. An Efficient Implementation of the Rainflow Counting Algorithm for Life Consumption Estimation. Ieee Transactions on Reliability. 2012;61(4):978-86.